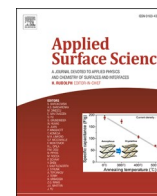




Contents lists available at ScienceDirect

Applied Surface Science

journal homepage: www.elsevier.com/locate/apsusc

Full Length Article

Fluorescence probing of binding sites on graphene oxide nanosheets with Oxazine 1 dye

Adrien Paudics^a, Shereen Farah^a, Imre Bertóti^b, Attila Farkas^c, Krisztina László^{a,*}, Miklós Mohai^b, György Sáfrán^d, András Szilágyi^a, Miklós Kubinyi^a^a Department of Physical Chemistry and Materials Science, Budapest University of Technology and Economics, Budapest H-1521, Hungary^b Institute of Materials and Environmental Chemistry, Research Centre for Natural Sciences, Eötvös Loránd Research Network, Magyar tudósok körútja 2., Budapest H-1117, Hungary^c Department of Organic Chemistry and Technology, Budapest University of Technology and Economics, Budapest H-1521, Hungary^d Research Institute for Technical Physics and Materials Science, Eötvös Loránd Research Network, Konkoly Thege M. út 29-33., Budapest H-1121, Hungary

ARTICLE INFO

Keywords:

Cationic dye

GO

Fluorescence detection

No need to separate supernatant

ABSTRACT

The adsorption of the fluorescent dye, Oxazine 1 (OX) was studied on graphene oxide (GO), in the range of low ($\leq 10^{-7}$ M) OX concentrations, exploiting the high sensitivity of fluorescence spectroscopy. Dry GO was characterized using XRD, TEM, XPS, Raman and IR spectroscopy, while its chemistry in aqueous suspension was examined with potentiometric titration. Adsorption isotherms were measured at pH 6.4 and 10.2 at temperatures 20 and 35 °C. All the isotherms were well described by the Langmuir equation. The saturation capacities n_m were higher at pH 10.2 than at 6.4 at the respective temperature, in accordance with the presence of additional dissociated acidic groups on the GO surface. The n_m values corresponded to a few percent occupancy of the dissociated acidic groups of GO. The equilibrium constant K_L for OX was substantially higher than the values reported for the adsorption of other cationic dyes from more concentrated solutions, indicating that our results refer to binding to the most active sites. The large negative adsorption enthalpy and the positive adsorption entropy are also indicative of strong binding interactions. In this case, probably the Coulomb interactions between the opposite charges on the adsorbent and adsorbate are dominant in the binding interactions.

1. Introduction

Although graphene oxide (GO) has been known since the middle of the 19th century [1], it has become a widely studied material only in the 21st century, following the successful preparation of single-layered graphene sheets [2]. Initially, GO served mainly as a convenient intermediate in the large-scale manufacture of graphene [3–5]. GO is a non-stoichiometric lattice of sp^2 and sp^3 hybrid state carbon atoms, with a large concentration of various oxygen containing functional groups on its surface (see Fig. 1). Hydroxy and epoxy groups are attached to the basal planes of GO sheets, whereas carboxyl, carbonyl, phenol, lactone and quinone groups are located at the edges [6]. GO is prepared by oxidation of graphite, and the chemical composition of the GO formed is determined by the quality of the graphite starting material and the reaction conditions [7,8]. GO has hydrophilic character [3,4] and it forms stable aqueous suspensions [9]. The stability of such suspensions is due partly to the increased separation, and hence weakened interactions,

between the GO sheets with oxygen containing groups on their surface, and partly to the formation of hydrogen bonds between the hydroxyl and carboxyl groups on the sheets and the water solvent molecules [3].

By now, owing to its tunable hydrophilic/hydrophobic character and easy processability in polar solvents, particularly in water, it has a wide range of applications in its own right. The variety of its functional groups makes GO a promising candidate for many applications [10–13]. Many different polymers and biomolecules can be bound to GO via the oxygen functional groups [14–17]. In this way, GO can function as a carrier for the transport of bioactive compounds [18]. Several applications of GO as catalysts [19,20] and adsorbents [21–23] in aqueous media have been reported. The functional groups also affect the electronic, mechanical and electrochemical properties of GO [24]. The concentration of defects in GO is much higher than in graphene, this may, however, be advantageous in some special applications in the semiconductor industry [4]. That GO is a photostable, non-toxic, biocompatible and environment-friendly material, has given rise to the development of many types of

* Corresponding author at: Műgyetem rkp. 3, Budapest 1111, Hungary.

E-mail address: klaszlo@mail.bme.hu (K. László).

<https://doi.org/10.1016/j.apsusc.2020.148451>

Received 7 September 2020; Received in revised form 6 November 2020; Accepted 9 November 2020

Available online 17 November 2020

0169-4332/© 2020 Elsevier B.V. All rights reserved.

GO-based optical biosensors and chemical sensors [25–30]. In the majority of GO-based fluorescent sensors reported so far, GO acted as the acceptor of a FRET-system (Förster resonance energy transfer), with quantum dots or an organic dye as donors [31]. As another fluorescence-related application, aptamer-conjugated GO-s have been prepared which functioned as fluorophores for NIR two-photon microscopic imaging [32,33].

In this work, the adsorption of a fluorescent indicator dye, Oxazine 1 (perchlorate salt, OX in Fig. 1) on GO has been investigated. Studying the adsorption of organic dyes is a straightforward means of characterizing the binding sites on GO nanosheets. Furthermore, the results may contribute to some technical applications of GO, e.g. the cleaning of industrial waste water with GO adsorbent or the development of GO based optical sensors. The adsorption of many dyes on GO [34–41], reduced GO [42] and GO composites [43] have been reported. Primarily, in these studies cationic dyes were the adsorbates, which interact strongly with the negatively charged GO nanosheets. In most cases, the surface coverage was determined by separating the solution phase and measuring the concentration of the unabsorbed dye by absorption spectroscopy [36,37]. In the case of fluorescent dyes, fluorescence quenching that accompanies the binding to GO provides a direct method for monitoring the adsorption process [38].

OX was chosen as the fluorescent probe in our study because (i) it absorbs in the red region of the visible spectrum, where GO absorbs very weakly; (ii) the fluorescent quantum yield of OX is relatively high in aqueous solution [44], and (iii) oxazine dyes have high pKa values: they are therefore present in the same protonation form (mono-protonated) over a wide pH range. Owing to the high sensitivity of fluorescence detection, samples with low dye and low GO concentrations could be used, and for this reason information was expected primarily on the interactions of the dye with the strongest binding sites. The adsorption process was characterized quantitatively by the Langmuir parameters, determined from the spectra of mixtures with constant GO and varied dye concentrations.

Prior to the fluorescence spectroscopic experiments, the structure of GO was characterized by powder X-ray diffraction (XRD), transmission electron microscopic imaging (TEM), X-ray photoelectron spectroscopy (XPS), infrared and Raman spectroscopic methods. A detailed thermogravimetric (TG) study of GO and its derivatives has been published recently [45]. The specific surface of GO was determined by nitrogen adsorption technique.

2. Materials and methods

GO was prepared from natural graphite powder (average particle size 63 μm) purchased from Graphite Týn (Týn nad Vltavou, Czech Republic) using the improved Hummers' method [46,47]. Oxazine 1, the fluorescent dye, was supplied by Sigma.

The powder X-ray diffraction (XRD) pattern of GO was measured with a PANalytical X'pert Pro MPD X-ray diffractometer using Cu K_{α} (1.54056 Å) radiation.

The morphology of the samples was characterized by a FEI Titan Themis 200 kV spherical aberration (Cs) corrected TEM 0.09 nm HRTEM and 0.16 nm STEM resolution equipped with 4 ThermoFischer "Super X G1" EDS detectors. The samples were drop-dried on TEM microgrids coated with ultrathin carbon layer.

Raman spectra were recorded with a LabRAM (Horiba Jobin Yvon) instrument having a $\lambda = 532$ nm Nd-YAG laser source (laser power at the focus point is 15 mW). Filter of 0.6 OD was used to reduce excitation beam energy reducing the chance of sample degradation. After baseline correction the first and second order regions of the spectrum were deconvoluted to Lorentzian functions using the conventional fitting procedures of the Origin program. The crystallite size (L_a) was estimated by the Tuinstra-Koenig-Cancado equation [48]

$$L_a = (2.4 \times 10^{-10} \text{ nm}^{-3}) \lambda^4 \left(\frac{I_D}{I_G}\right)^{-1} \quad (1)$$

The infrared spectra were recorded on a Tensor 37 (Brooker) FT-IR spectrometer in ATR mode. X-ray photoelectron spectra were recorded on a Kratos XSAM 800 spectrometer operating in fixed analyzer transmission mode, using Mg K_{α} (1253.6 eV) excitation. After subtraction of a Shirley type baseline, the quantitative analysis was performed by the Kratos Vision 2 and XPS MultiQuant programs.

For the potentiometric titration of GO, 0.05 g of the sample was suspended in 50 mL NaCl solution (0.01 M) at 25 °C. The suspension was titrated with 0.1 M NaOH solution in the pH window 3–10. The specific net proton surface excess was derived from the initial and equilibrium concentrations of the suspension [49,50].

The UV–Vis absorption spectra of the buffered GO suspensions were recorded on an Agilent 8453 single-beam spectrophotometer.

The samples used in the determination of the adsorption isotherms by fluorescence spectroscopy were GO-OX mixtures in Bis-Tris buffer of pH 6.4 and in CAPS buffer of pH 10.2. The samples were prepared by adding OX from a $2 \cdot 10^{-4}$ M stock solution to GO solutions of 2.5 mg/L. The equilibrium state (constant fluorescence intensity) of the stirred mixtures was reached typically in 30–60 min. The fluorescence spectra were acquired by an Edinburgh Instruments FS5 spectrofluorimeter. They were excited at 655 nm, at the absorption maximum of OX. The isotherms were measured at 20 and 35 °C.

3. Results and discussion

3.1. Characterization of GO in solid state

The X-ray diffractogram of GO is shown in Fig. 2, together with the diffractogram of natural graphite. The sharp peak of graphite at $2\theta = 26.3^\circ$ corresponds to an interlayer distance of 3.45 Å. With GO, however, the broader peak indicates a less regular structure: the position of the peak, $2\theta = 11.5^\circ$, yields for the interlayer spacing 7.73 Å. This larger spacing is the consequence of the oxygen substituents on the carbon skeleton.

HRTEM image (Fig. 3) reveals the heterogeneous layer structure of

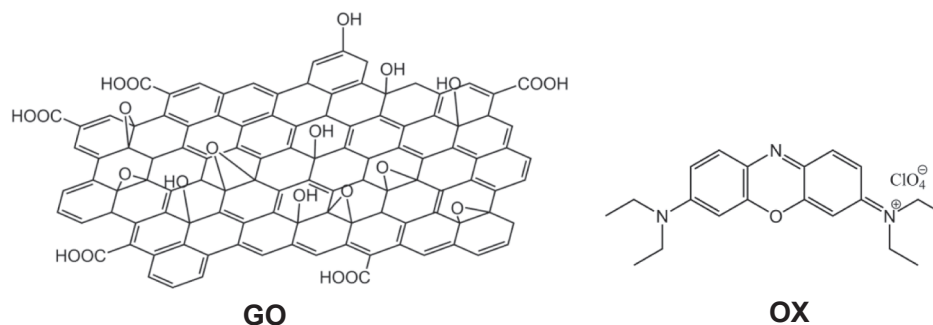


Fig. 1. The Lef-Klinowski model of graphene oxide (GO) and the chemical structures of Oxazine 1 (OX).

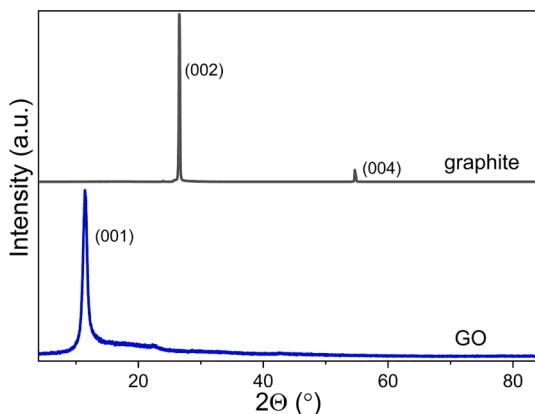


Fig. 2. X-ray diffractograms of graphite and GO.

the GO particles, in correlation with the diffractogram. The particles contain amorphous and polycrystalline regions (Fig. S1).

This was also confirmed by Raman spectroscopy (Fig. 4). Beside the iconic G ($\sim 1580\text{ cm}^{-1}$, graphitic band, related to the vibrations of the sp^2 building blocks) and D ($\sim 1350\text{ cm}^{-1}$, defect band, associated to structural disorder) bands the contribution of D' ($\sim 1600\text{ cm}^{-1}$, disordered graphitic lattices), D'' ($\sim 1506\text{ cm}^{-1}$, amorphous phases) and D* ($\sim 1220\text{ cm}^{-1}$, disorder from graphitic lattices and impurities) were recognized in the first order spectrum [51–53]. The second order region was assigned to the 2D ($\sim 2700\text{ cm}^{-1}$, structural order), 2D' combined G*, D + D' bands, the latter two in the 2300–3100 cm^{-1} region. These bands, their position and their relative intensities help to identify and characterize the chemical and physical properties of carbon materials [54,55]. In this paper we use the D, G and 2D bands for characterization, the latter being very sensitive to the stacking. The main structural parameters deduced from Raman spectroscopy are shown in Table 1.

It was found that in single-layer graphene the G and 2D bands usually appear at 1585 and 2679 cm^{-1} , and move to lower and higher Raman shift values, respectively, with increasing number of layers. The 2D/G ratio decreases with increasing number of layers (from >1.6 in single layer to 0.8, 0.30 and 0.07 by increasing the layer number to 2, 3 and 4, respectively) [56] and Refs. [66–72] within]. Indeed, in our sample the position of the bands shift in the expected directions. The I_{2D}/I_G ratio corresponds to a few layers on average, confirming the XRD and HRTEM observations.

The functional groups in bulk GO were identified by infrared spectroscopy (Fig. 5). The broad band in the 3000–3700 cm^{-1} corresponds to the ν_{OH} characteristic vibration, while the band at 1734 belongs to the $\nu_{\text{C=O}}$ vibrations of the carbonyl and carboxyl groups, the band at 1618 can be assigned to $\nu_{\text{arC-C}}$ modes (stretching modes of aromatic rings), and that at 1400 cm^{-1} belongs to the δ_{OH} bending modes of phenol and

tertiary alcohol groups. The feature at 1221 cm^{-1} arises from the $\nu_{\text{C-O}}$ (H) stretching vibrations. The band at 1054 cm^{-1} may originate from the $\nu_{\text{asC-O-C}}$ stretching modes of epoxide rings [57,58].

The photoelectron spectral regions of the C1s and O1s lines are shown in Fig. 6. The shapes of the lines are complex, indicating the presence of various chemical species on the surface. The C1s and O1s regions can be fitted with five and three components, respectively. The binding energies, the assignments of the components to chemical states and the quantitative compositions are shown in Table 2. This assignment is based on previous works and literature data; for details see Refs. [59–68] and Table S1.

The surface of GO is highly oxidized (28.5% total O). The proportions of the various oxidized carbon and oxygen species exhibit excellent agreement.

3.2. Characterization of GO in aqueous suspension

In the absorption spectrum of GO (Fig. 7a) the strong band at 230 nm arises from the $\pi \rightarrow \pi^*$ transitions of conjugated C=C units, while the

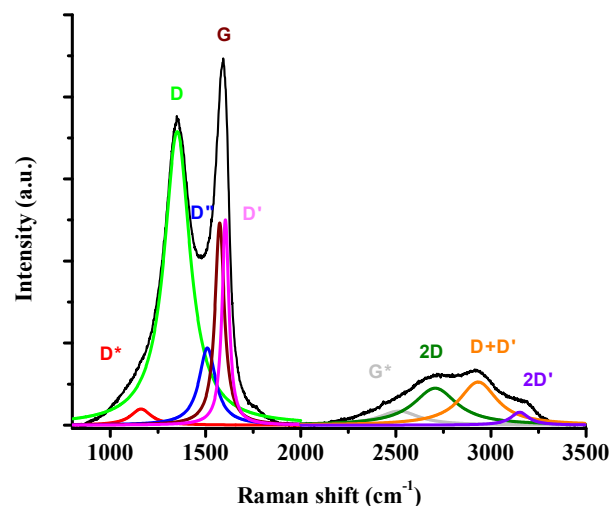


Fig. 4. Deconvoluted Raman spectrum of the dry GO sample.

Table 1
Parameters obtained from the deconvoluted Raman spectrum.

Carbon material	Raman shift (cm^{-1})			I_D/I_G	I_{2D}/I_G	L_n (nm)
	G-band	D-band	2D-band			
GO	1574	1351	2707	1.46	0.19	13.2

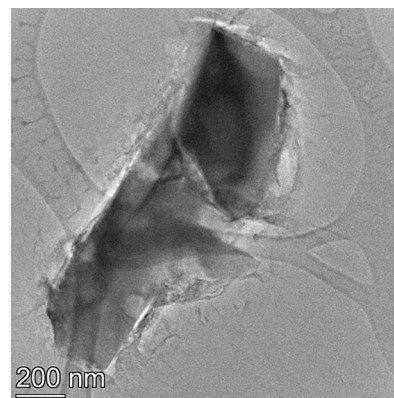
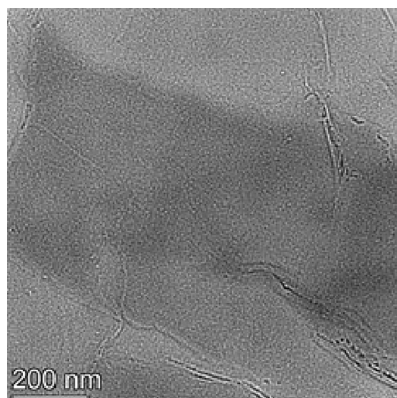


Fig. 3. HRTEM image of GO particles.

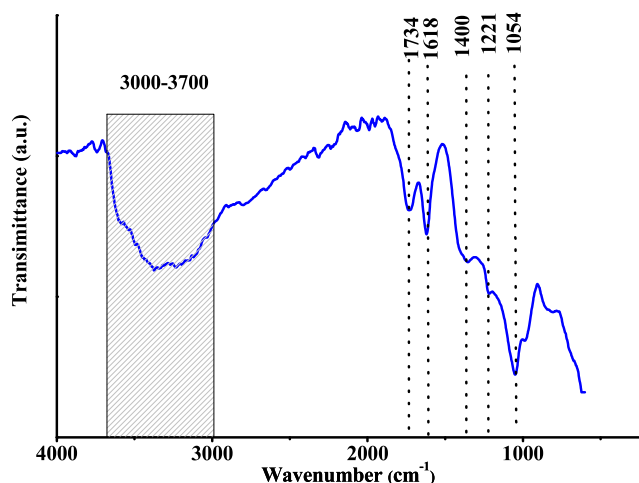


Fig. 5. ATR-FTIR spectrum of freeze-dried GO.

shoulder at 300 nm is assigned to the $n \rightarrow \pi^*$ transitions of C=O groups. The spectrum was found to obey Beer's law (inset in Fig. 7a), indicating that GO was fully dispersed into single layered sheets at the low concentrations employed in this study.

The fluorescence emission spectra (Fig. 7b) consist of distinct bands, with relative intensities depending on the excitation wavelength. On the basis of the excitation spectra (Fig. 7c), the fluorescence emission bands can be assigned to different aromatic structures decorated with C=O and other oxygen containing functional groups, embedded into a framework of sp^3 hybridized carbon atoms. Namely, the emission features around 300, 350 and 390 nm may be assigned to benzoic acid-like (or phenol-like), naphthoic acid-like and salicylic acid-like fluorescence centers, respectively [69].

The acid/base properties of the GO in dilute aqueous suspension were characterized by potentiometric titration in CO₂-free conditions. The pH of immersion was 2.98. The titration data were converted to a

proton excess isotherm (Fig. 8a), revealing that the surface is negatively charged in the whole pH range investigated. The increase in pH of the suspension leads to deprotonation of the various acidic functional groups decorating the graphene sheet. The SAIEUS procedure [70,71] was used to calculate the pK_a distribution and the concentration of the corresponding functional groups (Fig. 8b and Table 3). The good agreement between the XPS and titration results confirms that the majority of the functional groups is probably phenolic OH.

3.3. Spectral data of OX in aqueous solutions

The pK_a of OX was determined from the absorption spectra of the dye (Fig. S2 in the electronic supplementary information), measured between pH 9.7 and 14, yielding the value 11.74.

The spectral data of the protonated and neutral forms of OX are collected in Table 4. The adsorption experiments were carried out in buffers of 6.4 and 10.2, in which the protonated state dye was dominant. Comparing the spectra measured in the buffers to the spectra measured in neat water, the positions of the absorption and fluorescence bands did not change noticeably, whereas the fluorescent quantum yields were a little higher in the buffers. The detection limit of the dye in our fluorescence spectroscopic experiments was $\sim 5 \cdot 10^{-11}$ M.

3.4. Adsorption of OX on GO

The dye adsorption isotherms were determined at pH 6.4, where the negative charges of the GO nanosheets arise solely from dissociated carboxyl groups, and at pH 10.2 where all the acidic groups can be considered fully dissociated [9]. As mentioned above, the monocationic form of OX was dominant even at pH 10.2.

The pH 6.4 solutions were made in a Bis-Tris buffer, the pH 10.2 solutions in a CAPS buffer. The GO concentration was 2.5 mg/L in all the samples, and the dye concentration was varied between 0 and 1×10^{-7} M. Using such low dye concentrations, the absorbance of all the samples was below 0.015 in the range of the visible absorption band of OX. Thus, no correction of the fluorescence intensities for inner filter effects was

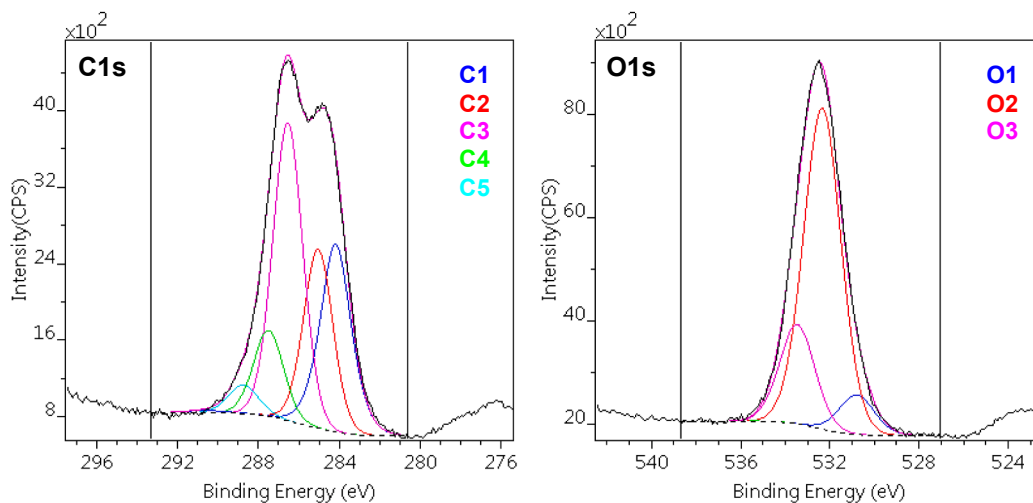


Fig. 6. C1s and O1s high resolution XP spectra of GO, decomposed into the bands of different chemical states.

Table 2

Binding energies (eV), assigned chemical states and surface chemical composition (atomic %) of GO calculated from XP spectra.

	O1	O2	O3	C1	C2	C3	C4	C5
Binding energy	530.8	532.4	533.5	284.2	285.1	286.6	287.5	288.8
Chemical states	C=O	C—O—C	O=C—O*	sp^2 C	sp^3 C	C—OH	C=O	O=C—O
	*O=C—OH	C—OH				C—O—C		
Composition	2.8	22.8	3.8	17.8	13.3	29.7	6.1	3.7

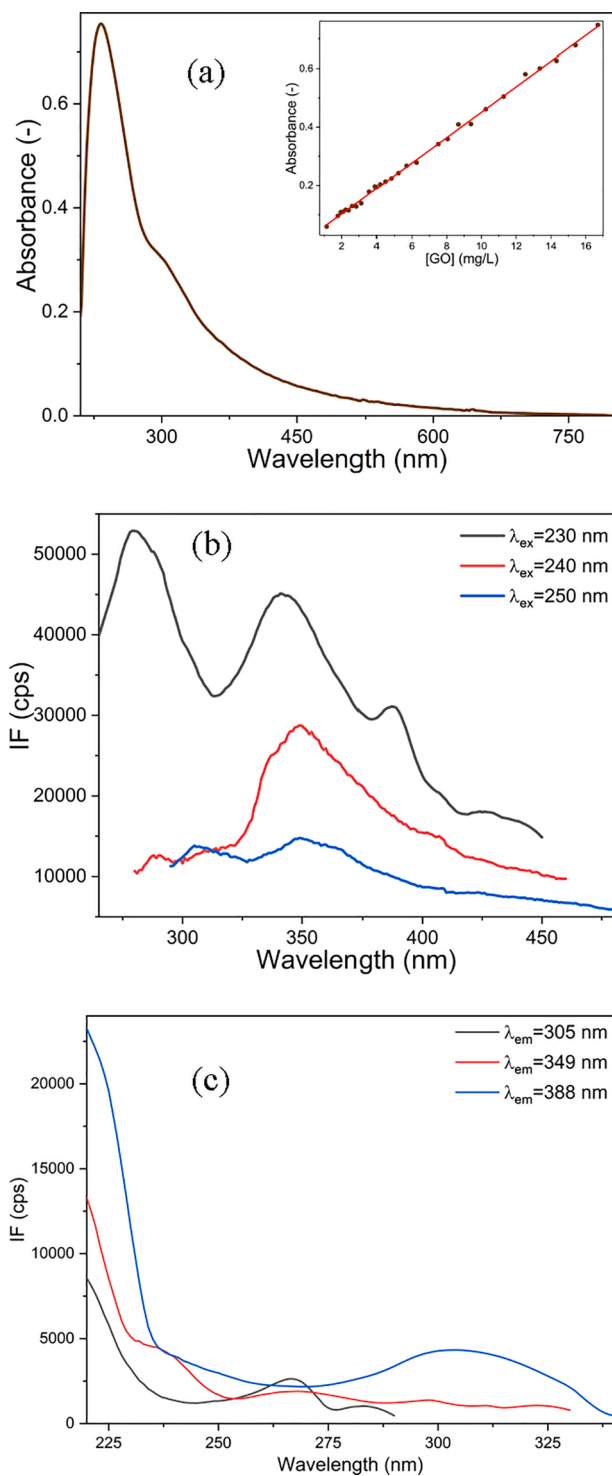


Fig. 7. (a) Absorption spectrum of GO in 18.8 mg/L aqueous suspension at pH = 6.4. The inset shows the calibration at $\lambda = 230$ nm; (b)–(c) fluorescence spectra in 0.57 mg/L aqueous suspension, pH = 6.4, (b) fluorescence emission spectra obtained at excitation wavelengths 230, 240 and 250 nm; (c) fluorescence excitation spectra obtained at emission wavelengths 305, 349 and 388 nm.

required. The isotherms were measured at 20 and 35 °C.

The fluorescence spectra of the GO-OX mixtures at the two pH values are illustrated in Fig. 9, displaying the spectra obtained at 20 °C. The amount of the adsorbed dye, n_s , was calculated for each sample from

$$n_s = \frac{(c_0 - c_e)V}{m_{ad}}, \quad (2)$$

where c_0 and c_e are the initial and equilibrium concentrations of the dye, calculated from the fluorescence intensities at 670 nm, the band maximum of OX (see insets in Fig. 9); m_{ad} is the mass of the dry adsorbent, V is the volume of the liquid phase. The adsorption isotherms are shown in Fig. 10.

The isotherms at both pH values and temperatures are of L Type [72]. Such isotherms have a well-defined plateau that is associated with the saturation capacity of the system. The isotherms were fitted to the hyperbolic form of the Langmuir model. The conditions of this model are (i) the binding sites are energetically homogeneous and (ii) the maximum amount of solute can be adsorbed in a monomolecular layer on the adsorbent. These assumptions lead to the isotherm equation with two parameters

$$n_s = \frac{n_m \cdot K_L \cdot c_e}{1 + K_L \cdot c_e} \quad (3)$$

Although the limits of the model are seldom strictly met, its great advantage is that it is based on a clear and simple physical model and the parameters can therefore be related directly to this physical picture: n_m is the adsorbed amount at full coverage (monolayer capacity) and K_L is the equilibrium constant of the adsorption.

The experimental data of all four isotherms conformed closely with the hyperbolic Langmuir equation with parameters K_L and n_m (for example, see the fitted functions in Fig. 10). The values of the two parameters are listed in Table 5.

On comparing the parameters obtained at pH = 6.4 and 10.2 at the same temperatures, the n_m adsorption capacities are higher in the more basic solutions, where a higher proportion of the acidic groups of GO are dissociated. Taking the ratios of the n_m values at 20 °C and the concentrations of the dissociated acidic groups from potentiometric titration, it can be concluded that the saturation condition corresponds to an occupancy of ~5% of the dissociated acidic groups of GO at pH 6.4, and an occupancy of ~1.5% of the dissociated acidic groups at pH 10.2. The values of the binding constants, K_L are also higher in the more basic samples. Furthermore, K_L decreases with increasing temperature – this holds both at pH 6.4 and 10.2. The latter trend indicates that the adsorption of the dye on the most active surface sites of GO is an exothermic process.

The Gibbs free energies of adsorption were obtained from the K_L values as

$$\Delta G = -RT \ln \left(\frac{K_L}{c^0} \right) \quad (4)$$

where K_L is expressed in units L/mol, $c^0 \equiv 1$ mol/L [73].

The values lie between –50 and –55 kJ/mol, which is higher than reported for similar systems in the case of physisorption (0–20 kJ/mol) but lower than the values characteristic of chemisorption, suggesting strong electrostatic interactions. The heats and entropies of adsorption estimated using the equation

$$\ln \left(\frac{K_L}{c^0} \right) = -\frac{\Delta H}{RT} + \frac{\Delta S}{R} \quad (5)$$

are shown in Table 6. The ΔH values indicate that the adsorption of OX on the most active binding sites of GO is strongly exothermic. The positive adsorption entropies show that the positive ‘solvent entropies’ overcompensate the negative ‘solute entropies’, as frequently occurs in aqueous systems [74,75]. In our case, the solvent entropy arises from the release of water molecules from the surface of GO nanosheets and the solvent shell of the dye molecules into the less ordered bulk water. The ‘solute entropy’ corresponds to the loss of the orientational and conformational freedom of the dye solute at the surface of the GO

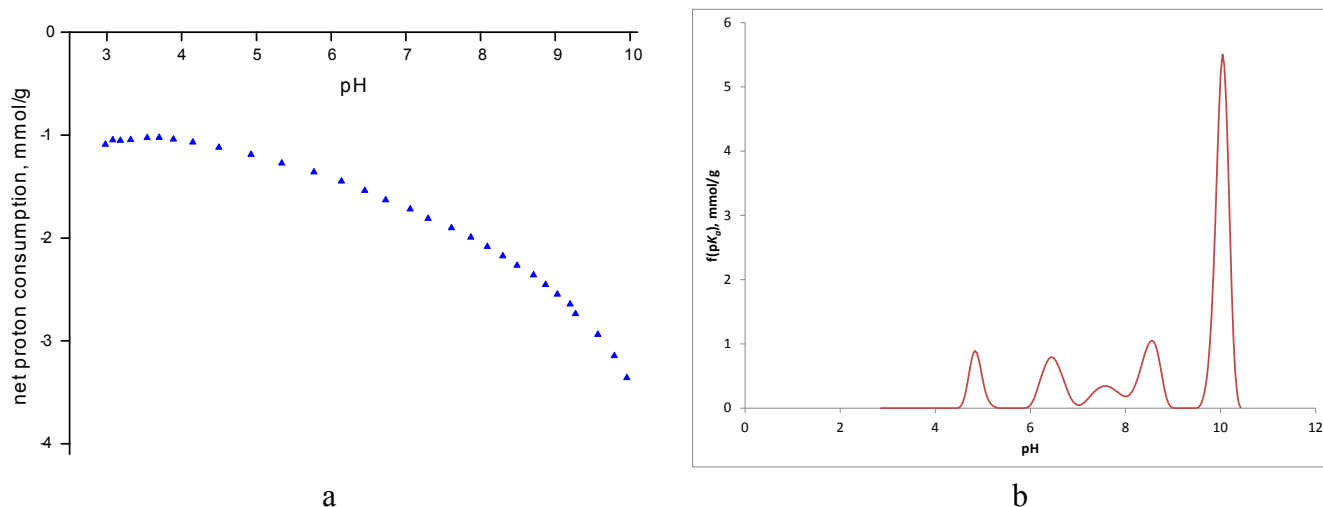


Fig. 8. The potentiometric titration curves of GO and the pK_a distribution calculated with SAIEUS program [71,72].

Table 3

Peak positions and quantification of the acidic groups.

	pK_a interval							Total
	3-4	4-5	5-6	6-7	7-8	8-9	9-10	
Peak maximum	–	4.85	–	6.46	7.58	8.50	10.03	
Concentration (mol/g)	–	$2.9 \cdot 10^{-4}$	–	$4.3 \cdot 10^{-4}$	$2.4 \cdot 10^{-4}$	$5.3 \cdot 10^{-4}$	$1.86 \cdot 10^{-3}$	$3.35 \cdot 10^{-3}$

Table 4

Absorption and fluorescence spectral data of OX in aqueous solutions^a.

Protonation state	Solvent	λ_{max}^{abs} [nm]	ϵ_{max} [$M^{-1}cm^{-1}$]	λ_{max}^F [nm]	Φ^F
Protonated	Neat water	655	$1.20 \cdot 10^5$	670	0.047
	Bis-tris buffer, pH 6.4	655	$1.25 \cdot 10^5$	670	0.054
	CAPS buffer, pH 10.2	655	$1.26 \cdot 10^5$	670	0.060
Neutral	1 M NaOH	675	$5.52 \cdot 10^4$	non-fluorescent	

^a Φ^F is the fluorescence quantum yield.

adsorbent.

On comparing the present results to the adsorption isotherms reported for other cationic dyes [34–36], the Langmuir model also provides a good description in most of the other cases. The low dye concentrations of our samples, sufficient for fluorescence detection,

allows us to gain information on binding to the most active sites on GO. The adsorption equilibrium constants obtained from these initial sections of the isotherms are significantly (10–100-times) higher than those reported for other cationic dyes, using higher dye concentrations. (For this comparison, the K_L values for the other dyes, expressed in L/(mg dye) by other groups, were converted into L/(mol dye) units.) There are examples for exothermic [41] as well as for endothermic [21,34] cationic dye adsorption on GO, noting again that much higher dye concentrations were used by the other groups.

The adsorption data may also be discussed at the molecular scale. If the adsorbed dye cations were oriented with their planes parallel with the basal planes of the GO nanosheets, the monolayer of OX cations would cover an area defined by

$$F_{GO} = N_A \cdot A_{OX} \cdot n_m \quad (6)$$

where N_A is Avogadro's number and A_{OX} is the cross sectional area of the dye cation. Taking the dimensions of OX cation from the quantum

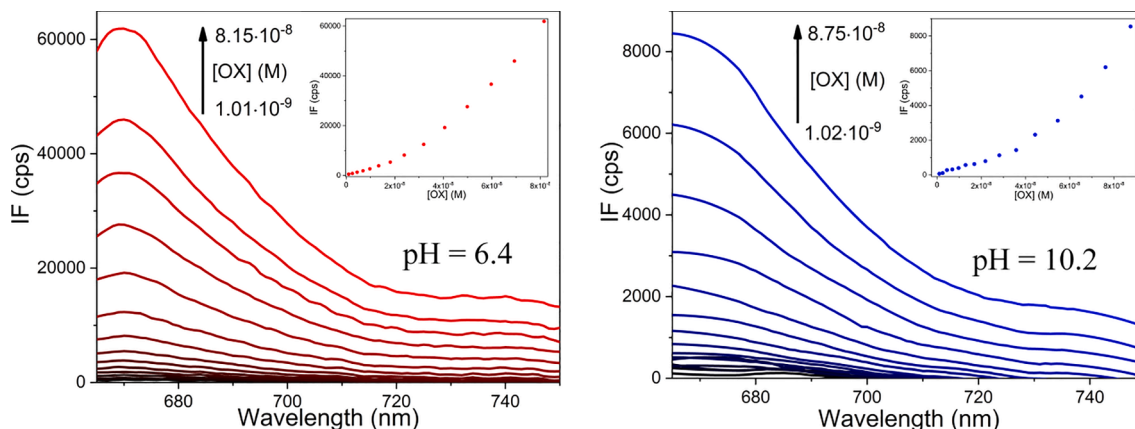


Fig. 9. Concentration dependence of the fluorescence spectra of OX in aqueous GO suspensions of 2.5 mg/L at pH = 6.4 and 10.2 at 20 °C. $\lambda_{ex} = 655$ nm.

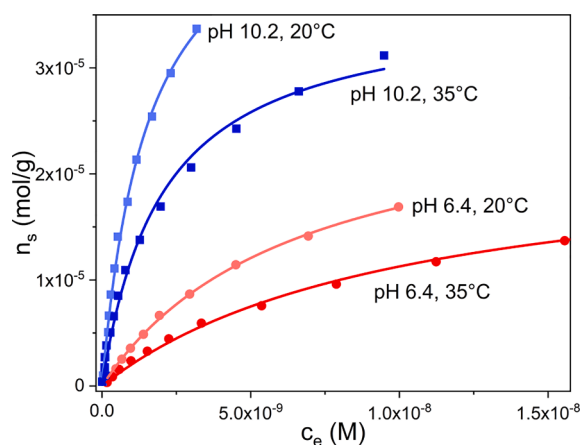


Fig. 10. Adsorption of OX on GO, measured in solutions of pH 6.4 and 10.2 at 20 °C and 35 °C. Symbols are the measured data. The solid lines represent the hyperbolic Langmuir fit.

Table 5
Parameters of Langmuir isotherms for the adsorption of OX on GO.

Isotherms	Temperature	n_m [mol/g]	K_L [L/mol]	R^2
pH 6.4	20 °C	$(2.8 \pm 0.1) \cdot 10^{-5}$	$(1.5 \pm 0.1) \cdot 10^8$	0.999
	35 °C	$(2.3 \pm 0.1) \cdot 10^{-5}$	$(9.8 \pm 0.5) \cdot 10^7$	0.998
pH 10.2	20 °C	$(5.0 \pm 0.2) \cdot 10^{-5}$	$(6.4 \pm 0.7) \cdot 10^8$	0.996
	35 °C	$(3.6 \pm 0.1) \cdot 10^{-5}$	$(4.9 \pm 0.5) \cdot 10^8$	0.993

Table 6
Thermodynamic data for the adsorption of OX on GO.

	ΔH [kJ/mol]	ΔS [J/(molK)]
pH 6.4	-39.6	78.0
pH 10.2	-15.7	119.3

chemical calculations in Ref. [76], namely $A_{OX} \sim 13 \text{ \AA} \times 6 \text{ \AA}$, and substituting the value of $2.8 \cdot 10^5 \text{ mol/g}$ for n_m (the value obtained at pH 6.4 and 20 °C), a surface area of $F_{GO} = 13 \text{ m}^2/\text{g}$ is obtained. This is $\sim 60\%$ of the surface area of the freeze-dried GO from nitrogen adsorption, $21 \text{ m}^2/\text{g}$.

The close agreement of these data is, however, misleading for several reasons. The OX and the N_2 adsorption characterize GO in different conditions: in very dilute well suspended state and as a freeze dried monolith. They also adsorb by different mechanisms, i.e., at adsorption sites of different type. First of all, the specific surface area of the GO nanosheets in their dilute aqueous suspension is certainly much greater than that of solid GO. Furthermore, it is unlikely that the adsorbed OX cations form a closely packed monolayer aligned with their plane parallel to the GO nanosheets, partly due to their diethyl substituted N regions and also owing to the epoxide oxygens randomly roughening the GO surface. From Raman spectroscopic observations of this GO it was found that the intensity ratio of the graphitic and defect peaks I_G/I_D is 1.18 ± 0.01 [45], which is an indication that the GO surface is severely damaged by the edge sites, the decorating O atoms and the carbon vacancies within the sheet.

The cross sectional area computed from quantum chemical considerations also ignores the water molecules attracted to OX. A further effect that may make the adsorption mechanism of OX more complicated – at least at higher OX concentrations – is that OX cations tend to form dimers at locations of high negative charge densities [77] and the edges of GO nanosheets are such positions.

Methylene blue is a well known and widely used cationic dye of very similar structure and more or less comparable molecular dimensions with a thickness of 4.7 \AA . Therefore, the area of the methylene blue dye

molecule with very similar chemical end geometrical structure, might be a good experimental estimate. It is 1.7 times larger than the OX area from quantum chemical calculations [78]. Even though with this concept we come even closer to the nitrogen surface area, any conclusion about a compact monolayer would be misleading.

The main molecular interactions might be i) the electrostatic attraction between the deprotonated functional groups of the GO and the positively charged N of the OX, and ii) the $\pi - \pi$ interactions between the quasi-aromatic regions of the adsorbent and the adsorbate. In view of the strong interaction it is more probable that they are bound to the negatively charged carboxylate units located at the edge of the GO nanosheets via electrostatic interactions. The geometry of the OX probe molecule and the high population of the deprotonated surface sites preclude a 1:1 correlation of the oppositely charged partners.

4. Conclusions

Our work on the adsorption of OX on GO demonstrates that the high sensitivity of fluorescence detection allows us to study the adsorption in the range of unusually low dye concentrations with only a limited amount of GO, and does not require separation of the “supernatant”. The adsorption isotherms were determined at pH 6.4 and 10.2 at temperatures 20 and 35 °C. They were all in good agreement with the Langmuir equation. The n_m saturation capacities corresponded to a few percent occupancy of the dissociated acidic functions of GO nanosheets by OX cations. The n_m values for OX were lower than those reported for the adsorption of other cationic dyes on GO, measured at similar pH values and temperatures, but on samples with higher dye concentrations. The K_L adsorption equilibrium constants were one or two orders of magnitude higher than the respective values for the adsorption of other cationic dyes from more concentrated solutions. This indicates that the adsorption from the dilute solutions is governed by the strong interactions at the most active binding sites of GO. The temperature dependence of the K_L values indicates that the adsorption of OX is an exothermic process. The results may contribute to the development of GO based optical sensors.

Declaration of Competing Interest

The authors declare that they have no known competing financial interests or personal relationships that could have appeared to influence the work reported in this paper.

Acknowledgement

The authors are grateful to J. Jagiello for kindly providing the SAIEUS program and to C. Ania for her contribution to pK_a distribution calculations. We acknowledge the help of J. Madarász for the XRD diffractogram and extend our warm thanks to G. Bosznai for his invaluable technical assistance.

Funding

This research was supported by the OTKA grants K 128410 and FK 125074 from National Research, Development and Innovation Office (NRDI). The research reported in this paper and carried out at BME has been supported by the NRDI Fund (TKP2020 IES, Grants BME-IE-BIO and BME-IE-NAT) based on the charter of bolster issued by the NRDI Office under the auspices of the Ministry for Innovation and Technology. A. Paudics thanks the Ministry for Innovation and Technology, Hungary, for the support by UNKP-19-3 New National Excellence Program. S. Farah is grateful to the Stipendium Hungaricum scholarship program, the Ministry of Higher Education and Research Sudan as well as University of Khartoum, Sudan for the financial support.

Appendix A. Supplementary material

Supplementary data to this article can be found online at <https://doi.org/10.1016/j.apsusc.2020.148451>.

References

- [1] B.C. Brodie, On the atomic weight of graphite, *Philos. Trans. Roy. Soc., Lond.* 149 (1859) 249–259, <https://doi.org/10.1098/rstl.1859.0013>.
- [2] K.S. Novoselov, A.K. Geim, S.V. Morozov, D. Jiang, Y. Zhang, S.V. Dubonos, I. V. Grigorieva, A.A. Firsov, Electric field effect in atomically thin carbon films, *Science* 306 (2004) 666–669, <https://doi.org/10.1126/science.1102896>.
- [3] S. Pei, H.M. Cheng, The reduction of graphene oxide, *Carbon* 50 (2012) 3210–3228, <https://doi.org/10.1016/j.carbon.2011.11.010>.
- [4] S. Park, R.S. Ruoff, Chemical methods for the production of graphenes, *Nat. Nanotechnol.* 4 (2009) 217–224, <https://doi.org/10.1038/nnano.2009.58>.
- [5] M.J. Fernández-Merino, L. Guardia, J.I. Paredes, S. Villar-Rodil, P. Solís-Fernández, A. Martínez-Alonso, J.M.D. Tascón, Vitamin C is an ideal substitute for hydrazine in the reduction of graphene oxide suspensions, *J. Phys. Chem. C* 6426 (6432) (114 2010), pp. 10.1021/jp100603h.
- [6] G. Eda, M. Chhowalla, Chemically derived graphene oxide: towards large-area thin-film electronics and optoelectronics, *Adv. Mater.* 22 (2010) 2392–2415, <https://doi.org/10.1002/adma.200903689>.
- [7] D.R. Dreyer, S. Park, C.W. Bielawski, R.S. Ruoff, The chemistry of graphene oxide, *Chem. Soc. Rev.* 39 (2010) 228–240, <https://doi.org/10.1039/B917103G>.
- [8] C. Hontoria-Lucas, A.J. López-Peinao, J.de D. López-González, M.L. Rojas-Cervantes, R.M. Martín-Aranda, Study of oxygen-containing groups in a series of graphite oxides: physical and chemical characterization, *Carbon* 33 (1995) 1585–1592, [https://doi.org/10.1016/0008-6223\(95\)00120-3](https://doi.org/10.1016/0008-6223(95)00120-3).
- [9] B. Konkena, S. Vasudevan, Understanding aqueous dispersibility of graphene oxide and reduced graphene oxide through pKa measurements, *J. Phys. Chem. Lett.* 3 (2012) 867–872, <https://doi.org/10.1021/jz300236w>.
- [10] L. Bacakova, J. Pajorova, M. Tomkova, R. Matejka, A. Broz, J. Stepanovska, S. Prazak, A. Skogberg, S. Siljander, P. Kallio, Applications of nanocellulose/nanocarbon composites: focus on biotechnology and medicine, *Nanomaterials* 10 (2020) 196–227, <https://doi.org/10.3390/nano10020196>.
- [11] P.T. Yin, S. Shah, M. Chhowalla, K.-B. Lee, Design, synthesis, and characterization of graphene–nanoparticle hybrid materials for bioapplications, *Chem. Rev.* 115 (2015) 2483–2531, <https://doi.org/10.1021/cr500537f>.
- [12] D. Chen, H. Feng, J. Li, Graphene oxide: preparation, functionalization, and electrochemical applications, *Chem. Rev.* 112 (2012) 6027–6053, <https://doi.org/10.1021/cr300115g>.
- [13] D. Plachá, J. Jampilek, Graphenic materials for biomedical applications, *Nanomaterials* 9 (2019) 1758–1794, <https://doi.org/10.3390/nano9121758>.
- [14] S. Bullo, K. Buskaran, R. Baby, D. Dorniani, S. Fakurazi, M.Z. Hussein, Dual drugs anticancer nanoformulation using graphene oxide-PEG as nanocarrier for protocatechuic acid and chlorogenic acid, *Pharm. Res.* 36 (2019) 91–101, <https://doi.org/10.1007/s11095-019-2621-8>.
- [15] O. Akhavan, E. Ghaderi, H. Emamy, Nontoxic concentrations of PEGylated graphene nanoribbons for selective cancer cell imaging and photothermal therapy, *J. Mater. Chem.* 22 (2012) 20626–20633, <https://doi.org/10.1039/c2jm34330d>.
- [16] S. Li, A.N. Aphale, I.G. Macwan, P.K. Patra, W.G. Gonzalez, J. Miksovská, R. M. Leblanc, Graphene oxide as a quencher for fluorescent assay of amino acids, peptides, and proteins, *ACS Appl. Mater. Interfaces* 4 (2012) 7069–7075, <https://doi.org/10.1021/am302704a>.
- [17] M. Zhang, B.-C. Yin, X.-F. Wang, B.-C. Ye, Interaction of peptides with graphene oxide and its application for real-time monitoring of protease activity, *Chem. Commun.* 47 (2011) 2399–2401, <https://doi.org/10.1039/C0CC04887A>.
- [18] H. Tiwari, N. Karki, M. Pal, S. Basak, R.K. Verma, R. Bal, N.D. Kandpal, G. Bisht, N. G. Sahoo, Functionalized graphene oxide as a nanocarrier for dual drug delivery applications: the synergistic effect of quercetin and gefitinib against ovarian cancer cells, *Colloids Surf. B* 178 (2019) 452–459, <https://doi.org/10.1016/j.colsurfb.2019.03.037>.
- [19] Z.M. Wang, K. Shishibori, K. Hoshino, H. Kanoh, T. Hirotsu, Examination of synthesis conditions for graphite-derived nanoporous carbon–silica composites, *Carbon* 44 (2006) 2479–2488, <https://doi.org/10.1016/j.carbon.2006.05.018>.
- [20] O. Akhavan, E. Ghaderi, S.A. Shirazian, Near infrared laser simulation of human neural stem cells into neurons on graphene nanomesh semiconductors, *Colloids Surf. B* 126 (2015) 313–321, <https://doi.org/10.1016/j.colsurfb.2014.12.027>.
- [21] T. Hartonoa, S. Wanga, Q. Mab, Z. Zhu, Layer structured graphite oxide as a novel adsorbent for humic acid removal from aqueous solution, *J. Coll. Interf. Sci.* 333 (2009) 114–119, <https://doi.org/10.1016/j.jcis.2009.02.005>.
- [22] A. Meidanchi, O. Akhavan, Superparamagnetic zinc ferrite spinel–graphene nanostructures for fast wastewater purification, *Carbon* 69 (2014) 230–238, <https://doi.org/10.1016/j.carbon.2013.12.019>.
- [23] H. Yan, H. Wu, K. Li, Y. Wang, X. Tao, H. Yang, A. Li, R. Cheng, Influence of the surface structure of graphene oxide on the adsorption of aromatic organic compounds from water, *ACS Appl. Mater. Interf.* 7 (2015) 6690–6697, <https://doi.org/10.1021/acsami.5b00053>.
- [24] C. Gómez-Navarro, J.C. Meyer, R.S. Sundaram, A. Chuvilin, S. Kurasch, M. Burghard, K. Kern, U. Kaiser, Atomic structure of reduced graphene oxide, *Nano Lett.* 10 (2010) 1144–1148, <https://doi.org/10.1021/nl9031617>.
- [25] P. Zheng, N. Wu, Fluorescence and sensing applications of graphene oxide and graphene quantum dots: a review, *Chem. Asian J.* 12 (2017) 2343–2353, <https://doi.org/10.1002/asia.201700814>.
- [26] C.I.L. Justino, A.R. Gomes, A.C. Freitas, A.C. Duarte, T.A.P. Rocha-Santos, Graphene based sensors and biosensors, *Trends Anal. Chem.* 91 (2017) 53–66, <https://doi.org/10.1016/j.trac.2017.04.003>.
- [27] J.-L. Chen, X.-P. Yan, K. Meng, S.-F. Wang, Graphene oxide based photoinduced charge transfer label-free near-infrared fluorescent biosensor for dopamine, *Anal. Chem.* 83 (2011) 8787–8793, <https://doi.org/10.1021/ac2023537>.
- [28] A.K. Akhila, N.K. Renuka, Coumarin–graphene turn-on fluorescent probe for femtomolar level detection of copper(II), *New J. Chem.* 43 (2019) 1001–1008, <https://doi.org/10.1039/C8NJ04732D>.
- [29] E. Morales-Narváez, A. Merkoçi, Graphene Oxide as an Optical Biosensing Platform, *Adv. Mater.* 24 (2012) 3298–3308, <https://doi.org/10.1002/adma.201200373>.
- [30] X. Deng, H. Tang, J. Jiang, Recent progress in graphene-material-based optical sensors, *Anal. Bioanal. Chem.* 406 (2014) 6903–6916, <https://doi.org/10.1007/s00216-014-7895-4>.
- [31] P.M. Neema, A.M. Tomy, J. Cyriac, Chemical sensor platforms based on fluorescence resonance energy transfer (FRET) and 2D materials, *Trends Analyt. Chem.* 124 (2020) 115797, <https://doi.org/10.1016/j.trac.2019.115797>.
- [32] A. Pramanik, S.R. Chavva, Z. Fan, S.S. Sinha, B. Priya, V. Nelloreand, P.C. Ray, Extremely high two-photon absorbing graphene oxide for imaging of tumor cells in the second biological window, *J. Phys. Chem. Lett.* 5 (2014) 2150–2154, <https://doi.org/10.1021/jz5009856>.
- [33] Z. Fan Pramanik, S.R. Chavva, S.S. Sinha, P.C. Ray, Highly efficient and excitation tunable two-photon luminescence platform for targeted multi-color MDRB imaging using graphene oxide, *Sci. Rep.* 4 (6090) (2014), <https://doi.org/10.1038/srep06090>.
- [34] W. Konicki, M. Aleksandrak, E. Mijowska, Equilibrium, kinetic and thermodynamic studies on adsorption of cationic dyes from aqueous solutions using graphene oxide, *Chem. Eng. Res. Des.* 123 (2017) 35–49, <https://doi.org/10.1016/j.cherd.2017.03.036>.
- [35] P. Bradder, S.K. Ling, S. Wang, S. Liu, Dye adsorption on layered graphite oxide, *J. Chem. Eng. Data* 56 (2011) 138–141, <https://doi.org/10.1021/je101049g>.
- [36] G.K. Ramesha, A.V. Kumara, H.B. Muralidhara, S. Sampath, Graphene and graphene oxide as effective adsorbents toward anionic and cationic dyes, *J. Colloid Interf. Sci.* 361 (2011) 270–277, <https://doi.org/10.1016/j.jcis.2011.05.050>.
- [37] S.-T. Yang, S. Chen, Y. Chang, A. Cao, Y. Liu, H. Wang, Removal of methylene blue from aqueous solution by graphene oxide, *J. Colloid Interf. Sci.* 359 (2011) 24–29, <https://doi.org/10.1016/j.jcis.2011.02.064>.
- [38] N. Kundu, A. Roy, D. Banik, J. Kuchlyan, N. Sarkar, Graphene oxide and pluronic copolymer aggregates—possible route to modulate the adsorption of fluorophores and imaging of live cells, *J. Phys. Chem. C* 119 (2015) 25023–25035, <https://doi.org/10.1021/acs.jpcc.5b05251>.
- [39] M. Rajabi, O. Moradi, M. Sillanpää, K. Zare, A.M. Asiri, S. Agarwal, V.K. Gupta, Removal of toxic chemical ethidiummonooxide bromide using graphene oxide: thermodynamic and kinetics study, *J. Mol. Liq.* 293 (2019) 111484–111493, <https://doi.org/10.1016/j.molliq.2019.111484>.
- [40] A.I. Abd-Elhamid, H.F. Aly, H.A.M. Soliman, A.A. El-Shanshory, Graphene oxide: follow the oxidation mechanism and its application in water treatment, *J. Mol. Liq.* 265 (2018) 226–237, <https://doi.org/10.1016/j.molliq.2018.05.127>.
- [41] S.-J. Song, Y.-F. Ma, H. Shen, M.-X. Zhang, Z.-J. Zhang, Removal and recycling of ppm levels of methylene blue from an aqueous solution with graphene oxide, *RSC Adv.* 5 (2015) 27922–27932, <https://doi.org/10.1039/C4RA16982D>.
- [42] H. Kim, S.-O. Kang, S.Y. Park, H.S. Park, Adsorption isotherms and kinetics of cationic and anionic dyes on three-dimensional reduced graphene oxide macrostructure, *J. Ind. Eng. Chem.* 21 (2015) 1191–1196, <https://doi.org/10.1016/j.jiec.2014.05.033>.
- [43] J.-Z. Sun, Z.H. Liao, R.-W. Si, G.P. Kingori, F.-X. Chang, L. Gao, Y. Shen, X. Xiao, X. Y. Wu, Y.-C. Yong, Adsorption and removal of triphenylmethane dyes from water by magnetic reduced graphene oxide, *Water Sci. Technol.* 70 (2014) 1663–1669, <https://doi.org/10.2166/wst.2014.427>.
- [44] X. Lv, C.M. Gao, T.H. Han, H. Shi, W. Guo, Improving the quantum yields of fluorophores by inhibiting twisted intramolecular charge transfer using electron-withdrawing group-functionalized piperidine auxochromes, *Chem. Commun.* 56 (2020) 715–718, <https://doi.org/10.1039/C9CC09138F>.
- [45] S. Farah, A. Farkas, J. Madarász, K. László, Comparison of thermally and chemically reduced graphene oxides by thermal analysis and Raman spectroscopy, *J. Therm. Anal. Calor.* (2020), <https://doi.org/10.1007/s10973-020-09719-3>.
- [46] W.S. Hummers, R.E. Offeman, Preparation of graphitic oxide, *J. Am. Chem. Soc.* 80 (1958), <https://doi.org/10.1021/ja01539a017>, 1339–1339.
- [47] D.C. Marcano, D.V. Kosynkin, J.M. Berlin, A. Sinitskii, Z. Sun, A. Slesarev, L. B. Alemany, W. Lu, J.M. Tour, Improved synthesis of graphene oxide, *ACS Nano* 4 (2010) 4806–4814, <https://doi.org/10.1021/nn1006368>.
- [48] L.G. Cancado, K. Takai, T. Enoki, General equation for the determination of the crystallite size L_a of nanographite by Raman spectroscopy, *Appl. Phys. Letters* 88 (2006) 163106, <https://doi.org/10.1063/1.2196057>.
- [49] K. László, E. Tombácz, K. Josepovits, Effect of activation on the surface chemistry of carbons from polymer precursors, *Carbon* 39 (2001) 1217–1228, [https://doi.org/10.1016/S0008-6223\(00\)00245-1](https://doi.org/10.1016/S0008-6223(00)00245-1).
- [50] H.D. Everett, Reporting data on adsorption from solution at the solid/solution interface, *Pure Appl. Chem.* 58 (1986) 967–984, <https://doi.org/10.1351/pac198658070967>.

- [51] A. Cuesta, P. Dhamelincourt, J. Laureyns, A. Martínez-Alonso, J.M.D. Tascón, Raman microprobe studies on carbon materials, *Carbon* 32 (1994) 1523–1532, [https://doi.org/10.1016/0008-6223\(94\)90148-1](https://doi.org/10.1016/0008-6223(94)90148-1).
- [52] S. Claramunt, A. Varea, D. López-Díaz, M.M. Velázquez, A. Cornet, A. Cirera, The importance of interbands on the interpretation of the Raman spectrum of graphene oxide, *J. Phys. Chem. C* 119 (2015) 10123–10129, <https://doi.org/10.1021/acs.jpcc.5b01590>.
- [53] S. Vollebregt, R. Ishihara, F.D. Tichelaar, Y. Hou, C.I.M. Beenakker, Influence of the growth temperature on the first and second-order Raman band ratios and widths of carbon nanotubes and fibers, *Carbon* 50 (2012) 3542–3554, <https://doi.org/10.1016/j.carbon.2012.03.026>.
- [54] X. Díez-Betriu, S. Alvarez-García, C. Botas, P. Álvarez, J. Sánchez-Marcos, C. Prieto, R. Menéndez, A. de Andrés, Raman spectroscopy for the study of reduction mechanisms and optimization of conductivity in graphene oxide thin films, *J. Mater. Chem. C* 1 (2013) 6905–6912, <https://doi.org/10.1039/C3TC31124D>.
- [55] D. López-Díaz, M. López Holgado, J.L. García-Fierro, M.M. Velázquez, Evolution of the Raman spectrum with the chemical composition of graphene oxide, *J. Phys. Chem. C* 121 (2017) 20489–20497, <https://doi.org/10.1021/acs.jpcc.7b06236>.
- [56] O. Akhavan, Bacteriorhodopsin as a superior substitute for hydrazine in chemical reduction of single-layer graphene oxide sheets, *Carbon* 81 (2015) 158–166, <https://doi.org/10.1016/j.carbon.2014.09.044>.
- [57] D. Yin, N. Lu, Z.-Y. Li, J.-L. Yang, A computational infrared spectroscopic study of graphene oxide, *J. Chem. Phys.* 139 (2013) 084704, <https://doi.org/10.1063/1.4818539>.
- [58] X. Jiao, Y. Qiu, L. Zhangab, X. Zhang, Comparison of the characteristic properties of reduced graphene oxides synthesized from natural graphites with different graphitization degrees, *RSC Adv.* 7 (2017) 52337–52344, <https://doi.org/10.1039/C7RA10809E>.
- [59] M. Mohai Bertóti, K. László, Surface modification of graphene and HOPG by nitrogen plasma: quantitative XPS analysis of chemical state alterations, *Carbon* 84 (2015) 185–196, <https://doi.org/10.1016/j.carbon.2014.11.056>.
- [60] H.K. Jeong, Y.P. Lee, R.J. Lahaye, M.H. Park, K.H. An, I.J. Kim, et al., Evidence of graphitic AB stacking order of graphite oxides, *J. Am. Chem. Soc.* 130 (2008) 1362–1366, <https://doi.org/10.1021/ja076473a>.
- [61] R. Larciprete, S. Gardonio, L. Petaccia, S. Lizzit, Atomic oxygen functionalization of double walled C nanotubes, *Carbon* 47 (2009) 2579–2589, <https://doi.org/10.1016/j.carbon.2009.05.008>.
- [62] I.-S. Byun, W. Kim, D.W. Boukhalval, I. Hwang, J.W. Son, G. Oh, et al., Electrical control of nanoscale chemical modification in graphene, *NPG Asia Mater.* 6 (2014) 102–107, <https://doi.org/10.1038/am.2014.24>.
- [63] J.-H. Zhou, Z.-J. Sui, J. Zhu, P. Li, D. Chen, Y.-C. Dai, et al., Characterization of surface oxygen complexes on carbon nanofibers by TPD, XPS and FT-IR, *Carbon* 45 (2007) 785–796, <https://doi.org/10.1016/j.carbon.2006.11.019>.
- [64] X. Xu, J. Zhu, Graphene–metal particle nanocomposites, *J. Phys. Chem. C* 112 (2008) 19841–19845, <https://doi.org/10.1021/jp807989b>.
- [65] A. Yang, G. Velamakanni, S. Bozoklu, M. Park, R.D. Stoller, Piner, et al., Chemical analysis of graphene oxide films after heat and chemical treatments by X-ray photoelectron and Micro-Raman spectroscopy, *Carbon* 47 (2009) 145–152, <https://doi.org/10.1016/j.carbon.2008.09.045>.
- [66] F. Liu, T. Seok Seo, A controllable self-assembly method for large-scale synthesis of graphene sponges and free-standing graphene films, *Adv. Funct. Mater.* 20 (2010) 1930–1936, <https://doi.org/10.1002/adfm.201000287>.
- [67] O. Akhavan, E. Ghaderi, A. Akhavan, Size-dependent genotoxicity of graphene nanoplatelets in human stem cells, *Biomaterials* 33 (2012) 8017–8025, <https://doi.org/10.1016/j.biomaterials.2012.07.040>.
- [68] A. Achour, S. Vizireanu, G. Dinescu, L. Le Brizoual, M.-A. Djouadi, M. Boujtita, Electrochemical anodic oxidation of nitrogen doped carbon nanowall films: X-ray photoelectron and Micro-Raman spectroscopy study, *Appl. Surf. Sci.* 273 (2013) 49–57, <https://doi.org/10.1016/j.apsusc.2013.01.112>.
- [69] Y. Kozawa, S. Mouri Miyauchi, K. Matsuda, Exploring the origin of blue and ultraviolet fluorescence in graphene oxide, *J. Phys. Chem. Lett.* 4 (2013) 2035–2040, <https://doi.org/10.1021/jz400930f>.
- [70] J. Jagiello, T.J. Bandosz, J.A. Schwarz, Carbon surface characterization in terms of its acidity constant distribution, *Carbon* 32 (1994) 1026–1028, [https://doi.org/10.1016/0008-6223\(94\)90066-3](https://doi.org/10.1016/0008-6223(94)90066-3).
- [71] J. Jagiello, Stable numerical solution of the adsorption integral equation using splines, *Langmuir* 10 (1994) 2778–2785, <https://doi.org/10.1021/la00020a045>.
- [72] J. Rouquerol, F. Rouquerol, P. Llewellyn, G. Maurin, K. Sing, *Adsorption by Powders and Porous Solids. Principles, Methodology and Applications*, second ed., Academic Press, 2013.
- [73] Y. Liu, Is the free energy change of adsorption correctly calculated? *J. Chem. Eng. Data* 54 (2009) 1981–1985, <https://doi.org/10.1021/je800661q>.
- [74] R.A. Singam, Y.-T. Zhang, G. Magnin, I. Miranda-Carvajal, L. Coates, R. Thakkar, H. Poblete, J. Comer, Thermodynamics of adsorption on graphenic surfaces from aqueous solution, *J. Chem. Theory Comput.* 15 (2019) 1302–1316, <https://doi.org/10.1021/acs.jctc.8b00830>.
- [75] M.F. Li, Y.-G. Liu, G.-M. Zeng, S.-B. Liu, X.-J. Hu, D. Shu, L.-H. Jiang, X.-F. Tan, X.-X. Cai, Z.-L. Yan, Tetracycline adsorbed onto nitrilotriacetic acid-functionalized magnetic graphene oxide: influencing factors and uptake mechanism, *J. Coll. Interface Sci.* 485 (2017) 269–279, <https://doi.org/10.1016/j.jcis.2016.09.037>.
- [76] M. Sayed, M. Sundararajan, J. Mohanty, A.C. Bhasikuttan, H. Pal, Photophysical and quantum chemical studies on the interactions of oxazine-1 dye with cucurbituril macrocycles, *J. Phys. Chem. B* 119 (2015) 3046–3057, <https://doi.org/10.1021/jp509243j>.
- [77] M. Kubinyi, T. Vidóczy, O. Varga, K. Nagy, I. Bitter, Adsorption and fluorescence spectroscopic study on complexation of oxazine 1 dye by calix[8]arenesulfonate, *Appl. Spectrosc.* 59 (2005) 134–139, <https://doi.org/10.1366/0003702052940477>.
- [78] J.J. Kipling, *Adsorption from Solutions of Non-Electrolytes*, Academic Press, London, 1965.